Annals of Pharmacy Practice and Pharmacotherapy
ISSN: 3062-4436
2021, Volume 1, Page No: 144-160

Available online at: www.galaxypub.co/page/journals

Galaxy Publication

Galaxy Publication

Potential Anti-Pneumonia Bioactive Compounds of Glycyrrhizae Radix et Rhizoma Following Gan An He Ji Oral Liquid Treatment

Sophia Davies[1]*, William Brown[1], Emma Wilson[1]

[1]Department of Pharmacology, Faculty of Life Sciences, University of Manchester, Manchester, UK.

***E-mail** ✉ sophia.davies@gmail.com

Received: 16 August 2021; **Revised:** 21 November 2021; **Accepted:** 21 November 2021

ABSTRACT

Glycyrrhizae Radix et Rhizoma, commonly known as Gan Cao (GC), is widely used in traditional Chinese medicine formulations for pneumonia management, yet its active pharmacological constituents in this context remain largely uninvestigated. Gan An He Ji oral liquid (GAHJ), a clinically used preparation composed of GC extracts and paregoric, was selected as a model compound to explore GC's therapeutic components for pneumonia. In a clinical study, patients with pneumonia received GAHJ treatment for three days, and intelligent mass spectrometry-based data analysis was employed to characterize GC metabolism in vivo. This approach identified 168 GC-related compounds in humans, including 24 prototype compounds and 144 metabolites, of which 135 detected in plasma and 82 in urine. By assessing metabolic transformation patterns and relative systemic exposure, six compounds—liquiritin, liquiritigenin, glycyrrhizin, glycyrrhetinic acid, daidzin, and formononetin—were proposed as potential active components. Experimental validation using two animal pneumonia models and an inflammatory cell model demonstrated that the combination of these six compounds alleviated pneumonia and lung injury while significantly reducing inducible nitric oxide synthase (iNOS) levels. Notably, glycyrrhetinic acid showed the highest in vivo exposure and the strongest iNOS inhibitory effect, which was further supported by molecular dynamics simulations revealing a stable interaction between glycyrrhetinic acid and iNOS. Overall, this study provides a pharmacological rationale for GC and elucidates potential mechanisms underlying its efficacy in pneumonia treatment.

Keywords: Glycyrrhetinic acid, Inducible nitric oxide synthase, Active components, Pneumonia, Glycyrrhizae Radix et Rhizoma

How to Cite This Article: Davies S, Brown W, Wilson E. Potential Anti-Pneumonia Bioactive Compounds of Glycyrrhizae Radix et Rhizoma Following Gan An He Ji Oral Liquid Treatment. Ann Pharm Pract Pharmacother. 2021;1:144-60. https://doi.org/10.51847/EKlViUjMo4

Introduction

Glycyrrhizae Radix et Rhizoma, widely recognized as Gan Cao (GC), is a traditional Chinese medicine (TCM) derived mainly from the roots of Glycyrrhiza inflata Bat., Glycyrrhiza glabra L., and Glycyrrhiza uralensis Fisch. [1-3]. It is extensively incorporated into clinical TCM prescriptions, with reports indicating that nearly 60% of these prescriptions include GC [1, 3]. GC exhibits a range of pharmacological activities, including antibacterial, anti-inflammatory, antiviral, and anti-tumor effects [4-7], which have led to its clinical application in treating conditions such as cough, bronchitis, peptic ulcers, and dermatitis [8-11]. Since the emergence of COVID-19, GC has been recognized as an effective component in several TCM formulations, including Qingfei Paidu decoction, Huashi Baidu prescription, Xuanfei Baidu prescription, and Lianhua Qingwen capsules [12-17]. Previous studies on GC for pneumonia treatment have predominantly focused on its general pharmacological effects or the mechanistic roles of specific active monomeric components—for instance, glycyrrhizin, which can inhibit SARS-CoV-2 replication by targeting the angiotensin-converting enzyme 2 receptor [18]. Nevertheless, investigations into the in vivo exposure profile and the identification of GC constituents specifically effective against respiratory diseases such as pneumonia remain limited.

Chinese herbal medicines typically display "multi-component, multi-target, and multi-functional" therapeutic properties [19], which complicates the identification of their active ingredients and mechanisms of action. Most TCMs are administered orally, and aside from components modulating intestinal microbiota, the therapeutic effects largely depend on prototype compounds or metabolites that achieve bioactive concentrations in vivo. Therefore, evaluating actual human exposure can enhance the efficiency of screening for pharmacologically active TCM constituents [20-22].

This study aimed to systematically identify GC-related compounds present in vivo in pneumonia patients after administration of TCM formulations, utilizing ultra-high-performance liquid chromatography–high-resolution mass spectrometry (UPLC-HRMS) coupled with advanced mass spectrometry data-mining techniques. To comply with ethical requirements for human studies, only commercially approved TCM formulas with GC as a primary component and indicated for respiratory inflammation by the National Medical Products Administration (Beijing, China) were considered. Gan An He Ji oral liquid (GAHJ), consisting of GC extract and paregoric, was selected as a representative prescription, given its clinical efficacy in alleviating cough and resolving phlegm in patients with various types of pneumonia. Its simple formulation minimizes interference from other components, facilitating the identification of potentially active GC constituents.

The primary objectives of this study were to map the in vivo exposure of GC and pinpoint potential active compounds using intelligent MS data-mining and metabolic profiling. In addition, absorption, distribution, metabolism, and excretion (ADME) analyses were conducted in rats to better understand the metabolic clearance of key GC components. From an action-mechanism perspective, candidate bioactive compounds were further analyzed through "compound-disease-target" network pharmacology, molecular modeling to predict potential protein targets, and systematic pharmacological validation in cell models and animal pneumonia models to confirm the therapeutic potential of GAHJ in pneumonia treatment.

Materials and Methods

Chemicals and materials

The following reagents and materials were employed in this study: magnoflorine, liquiritin, ononin, daidzein, liquiritigenin, calycosin, formononetin, isoliquiritigenin, glycyrrhizin, and glycyrrhetinic acid (purity ≥98%; Baoji Chenguang Biological Co., Ltd., Baoji, China); blank Sprague-Dawley (SD) rat plasma (Shanghai Yuanye Bio-Technology Co., Ltd., Shanghai, China); Oasis® HLB solid-phase extraction columns (6 mL/500 mg; Waters, Milford, MA, USA); HPLC-grade methanol and acetonitrile (Tedia High-Purity Solvents, Fairfield, OH, USA); LCMS/HPLC-grade formic acid (Anaqua™ Chemicals Supply, Wilmington, DE, USA); normal saline (ChenXin Biology Co., Ltd., Jining, China); heparin sodium (Shanghai Aladdin Bio-Chem Technology Co., Ltd., Shanghai, China); lipopolysaccharide (LPS) (Beijing Solarbio Science & Technology Co., Ltd., Beijing, China); anti-inducible nitric oxide synthase (iNOS) antibody and tumor necrosis factor receptor II (Abcam, Cambridge, UK); mouse iNOS and TNF-α ELISA kits (Wuhan Fine Test Biotech Co., Ltd., Wuhan, China); Hieff® qPCR SYBR Green Master Mix (Low Rox Plus), Hifair® II 1st Strand cDNA Synthesis SuperMix for qPCR (gDNA digester plus), TRIeasy™ Total RNA Extraction Reagent (Yeasen Biotechnology (Shanghai) Co., Ltd., Shanghai, China); 10% polyacrylamide gel electrophoresis (PAGE) gel quick preparation kit (Suzhou NCM Biotech Co., Ltd., Suzhou, China); protease inhibitor cocktail (MedChemExpress, Monmouth Junction, NJ, USA); iNOS rabbit polyclonal antibody and 10–180 kDa protein marker (Wuhan ABclonal Biotechnology Co., Ltd., Wuhan, China); 1400W (Selleck, Shanghai, China); and ultrapure water produced using a Milli-Q purification system (Merck KGaA, Darmstadt, Germany).

Collection of clinical samples

This study was approved by the Medical Ethics Committee of the First Affiliated Hospital of Xiamen University (Approval No.: [2020] Scientific Research Ethics Review [053]; Xiamen, China). A single-center, open-label, randomized clinical trial was conducted, enrolling three male patients diagnosed with pneumonia. Written informed consent was obtained from all participants prior to their inclusion.

Animal studies

Male Sprague-Dawley rats (200–220 g) and C57BL/6 mice (18–20 g) were sourced from the Laboratory Animal Center at Xiamen University. All animal procedures adhered to the institutional guidelines and were approved by the Animal Ethics Committee of Xiamen University (Approval No.: XMULAC20210116).

Drug administration and sample collection in rats

Rats (n = 6) were administered GAHJ orally at a dose of 20 mL/kg. Three rats were individually housed in metabolic cages for the collection of baseline plasma, urine, and fecal samples 12 hours before administration. GAHJ was then administered once daily for seven consecutive days, with subsequent collection of blood, urine, and feces. The remaining three rats were designated for bile collection.

Pneumonia model establishment and sample collection

LPS-Induced pneumonia mouse model

Mice were randomly assigned to four groups, each consisting of 10 animals: control (CON), model (LPS), pharmacodynamic component treatment (LPS-Mix), and GAHJ treatment (LPS-GAHJ). Pneumonia was induced via intranasal administration of LPS at 50 μL per mouse. Group details were as follows: normal mice with healthy lungs (CON); mice with pneumonia induced by 10 mg/kg LPS and treated with normal saline (LPS) [23, 24]; mice with 10 mg/kg LPS-induced pneumonia receiving 0.3 mL of the pharmacodynamic component (LPS-Mix); and mice with 10 mg/kg LPS-induced pneumonia treated with 0.3 mL of GAHJ (LPS-GAHJ). Following LPS induction for 24 hours, the treatment was administered once every 24 hours for 7 consecutive days. On day 8, serum and lung tissue samples were collected for analysis.

Staphylococcus aureus (s. Aureus)-induced pneumonia mouse model

Mice were similarly divided into four groups (CON, model [S. aureus], pharmacodynamic component treatment [S. aureus-Mix], and GAHJ treatment [S. aureus-GAHJ]) with 10 mice per group. Pneumonia was induced through intranasal administration of S. aureus (OD600 = 0.1) at 50 μL per mouse [25]. The group assignments and treatments mirrored those described for the LPS-induced model.

Sample preparation

Preparation of GAHJ test samples

GAHJ was filtered using a 0.22-μm pore size membrane before analysis.

Pretreatment of plasma, urine, and bile samples

Plasma samples collected at various time points post-administration were combined. These samples were diluted threefold with ultrapure water and then subjected to enrichment and purification using an Oasis® HLB column. Blank plasma samples were processed using the same procedure.

Urine and bile samples collected from 0 to 24 hours post-administration were pooled and similarly processed with the Oasis® HLB column. Blank urine and bile samples from rats underwent identical pretreatment.

After enrichment, methanol eluents were collected and evaporated under a nitrogen stream. The residues were reconstituted in 70% methanol, followed by brief sonication (10 s), vortexing, and centrifugation at 12,000 rpm for 10 minutes (D3024, DLAB Scientific Co., Ltd., Beijing, China) to obtain the supernatant for subsequent analysis.

Pretreatment of rat fecal samples

Fecal samples from rats, collected within 0–24 hours after GAHJ administration, were pooled and extracted with three volumes of ultrapure water and methanol.

UPLC-HRMS analysis

Analysis was performed using a Thermo Fisher Q Exactive Orbitrap mass spectrometer (Thermo Fisher Scientific Inc., Waltham, MA, USA). The mobile phases were water containing 0.1% formic acid (A) and acetonitrile (B). Separation was achieved on an ACQUITY UPLC CSH C18 column (2.1 mm × 50 mm, 1.7 μm; Waters, Milford, MA, USA) at 30 °C with a flow rate of 0.3 mL/min. Gradient elution was set as follows: 0–2 min (2% B), 2–10 min (2–10% B), 10–12.5 min (10–15% B), 12.5–16.5 min (15–20% B), 16.5–19.5 min (20–30% B), 19.5–21.5 min (30–35% B), 21.5–23.5 min (35–95% B), 23.5–28 min (95% B), 28–28.1 min (95–2% B), and 28.1–33.1 min

(2% B). UV detection was performed at 205, 254, and 310 nm, with injection volumes of 1 μL for GAHJ and three μL for samples.

Mass spectrometry parameters were set as follows: full MS resolution 35,000; scan range m/z 100–1200; dd-MS2 resolution 17,500; (N) CE/stepped (N) CE 35%; spray voltage +3.8 kV / −3.5 kV; capillary temperature 320 °C; sheath gas (N2) 35 arb; sweep gas (N2) 5 arb; auxiliary gas (N2) 10 arb.

Network pharmacology

For the efficacy prediction in this study, compounds exhibiting high bioavailability after GAHJ administration were selected. Each compound name was used as a query to identify seed genes through the Traditional Chinese Medicine Systems Pharmacology Database and Analysis Platform (TCMSP, http://tcmspw.com/tcmsp.php) and SwissTargetPrediction (http://www.swisstargetprediction.ch/). After removing duplicate entries, a refined "drug-target" dataset was obtained. To determine pneumonia-related targets, the Comparative Toxicogenomics Database (CTD, http://ctdbase.org/) was queried using "Pneumonia" as the search term. Overlapping targets were further analyzed by constructing a protein-protein interaction (PPI) network via the STRING database (https://string-db.org/cgi/input.pl), with a high confidence cutoff of 0.700. Network visualization and identification of the top 100 key proteins were performed using Cytoscape v3.7.2. Finally, detailed molecular network analysis was conducted employing the ClueGO plug-in within Cytoscape.

Molecular docking

Docking simulations were carried out using GOLD (Genetic Optimization for Ligand Docking, version 5.2) [26], a molecular docking software from the Cambridge Crystallographic Data Centre. Crystal structures of the predicted targets were obtained from the Protein Data Bank (PDB), and the ligand-binding sites were defined based on co-crystallized ligands. Each ligand was docked ten times, starting with distinct random orientations, under default automatic genetic algorithm parameters.

Immunohistochemistry (IHC) analysis

The middle lobe of the right lung from pneumonia model mice was fixed in 4% tissue fixative, embedded in paraffin, and sectioned at four μm thickness. Sections were dewaxed and incubated overnight at 4 °C with primary antibodies against iNOS (ab15323, 1:100) and TNF-α (ab109322, 1:150). Chromogenic staining was used to evaluate protein expression, with yellow indicating low and brown indicating high expression. Observations were made under a biological microscope (Olympus BX53, Olympus Corporation, Miyazaki, Japan).

Serum analysis of iNOS and TNF-α

Concentrations of iNOS and TNF-α in serum were determined using respective ELISA kits. Absorbance was measured at 450 nm with a microplate reader, and analyte levels were quantified via standard curves.

Quantitative real-time PCR (qRT-PCR)

Lung tissues were harvested from experimental mice and stored at −80 °C. Total RNA was extracted using Trizol reagent and dissolved in 20 μL diethyl pyrocarbonate-treated water for storage at −80 °C. Each qRT-PCR reaction (20 μL) contained one μL DNA template, 10 μL Hieff® qPCR SYBR® Green Master Mix (Low Rox Plus), 0.4 μL of each 10 μM primer, and 8.2 μL ultrapure water. The cycling protocol included an initial denaturation at 95 °C for 5 min, followed by 40 cycles of 95 °C for 10 s and 60 °C for 30 s. Reactions were analyzed using the Agilent AriaMx system (Agilent Technologies Co., Ltd., Palo Alto, CA, USA). Primers were as follows: GAPDH (F: CCTTCCGTGTTCCTACCC; R: CAACCTGGTCCTCAGTGTAG), iNOS (F: GGTGAAGGGACTGAGCTGTT; R: ACGTTCTCCGTTCTCTTGCAG), and TNF-α (F: CTTCTCATTCCTGCTTGTG; R: ACTTGGTGGTTTGCTACG). Relative expression levels of iNOS and TNF-α were calculated using the 2^−ΔΔCT method, with GAPDH as the endogenous control.

RAW264.7 cell culture

Mouse macrophage RAW264.7 cells were maintained in Dulbecco's Modified Eagle Medium (DMEM; Gibco, Carlsbad, CA, USA) supplemented with 20% fetal bovine serum and 1% penicillin-streptomycin. Cultures were incubated at 37 °C in a humidified atmosphere containing 5% CO_2.

Cell viability assay

Cytotoxic effects were assessed using the MTT (3-(4,5-dimethylthiazol-2-yl)-2,5-diphenyltetrazolium bromide) assay. RAW264.7 cells were seeded in 96-well plates at a density of 1×10^5 cells per well and treated with the test compounds. After 24 hours, the medium was replaced with MTT solution and incubated for an additional 4 hours. Subsequently, 150 μL of dimethyl sulfoxide (DMSO) was added to dissolve the formazan crystals, and the absorbance at 490 nm was recorded using a microplate reader (CMax Plus, Molecular Devices, San Francisco, CA, USA).

Nitric oxide synthase (NOS) activity

RAW264.7 cells were stimulated with LPS (1 μg/mL) for 24 hours to induce a proinflammatory response [27, 28]. Test compounds, including monomeric active components at varying concentrations, were co-administered with LPS. NOS activity was measured using a commercial NOS assay kit in conjunction with a selective iNOS inhibitor.

Western blotting (WB)

Cells (1×10^5 per well) were cultured in six-well plates for 12 hours before treatment with monomer compounds at designated concentrations in medium containing 1 μg/mL LPS for 24 hours. After washing with cold phosphate-buffered saline (PBS), proteins were extracted using 200 μL lysis buffer containing 1% protease inhibitor. Extracted proteins were denatured in SDS, separated via SDS-PAGE, and transferred to nitrocellulose membranes. Membranes were blocked at room temperature in 5% skim milk in Tris-buffered saline with 0.1% Tween-20 (TBST) for 1 hour to prevent nonspecific binding. Membranes were then incubated overnight at 4 °C with primary antibody against iNOS (Cat. No.: A0312, 1:1000). After washing with TBST, membranes were treated with HRP-conjugated secondary antibodies (anti-rabbit or anti-mouse IgG) for 1 hour. Protein signals were visualized using enhanced chemiluminescence reagents, and relative band intensities were quantified with ImageJ software.

Molecular dynamics (MD) simulation

The crystal structure of human iNOS in complex with the inhibitor AR-C9579 (PDB ID: 3E7G) was obtained [29] and used as a reference for GOLD molecular docking. The glycyrrhetinic acid-iNOS complex obtained from docking was subsequently subjected to MD simulation. For iNOS, two cofactors, protoporphyrin IX containing Fe (HEM) and tetrahydrobiopterin (H4B), were included to replicate physiological conditions. H4B forms a hydrogen bond with the propionate group of HEM's A ring, donating an electron crucial for dioxygen activation during catalysis [30, 31]. While H4B is not required for dimer formation, it stabilizes the iNOS dimer via interactions with both subunits [32]. Since HEM and H4B are located near the active site, both were retained in simulations.

Geometries of HEM, H4B, and glycyrrhetinic acid were optimized using Gaussian16 with B3LYP/6-31G* basis set, and partial charges were assigned via restrained electrostatic potential fitting. The system was solvated explicitly in a truncated octahedral TIP3P water box using the Amber ff14SB and generalized Amber force fields, with counterions added for charge neutrality. After energy minimization and equilibration following standard protocols [33], a 100-ns MD simulation was performed under NPT ensemble conditions (T = 300 K, P = 1 atm). Nonbonded interactions were truncated at 8 Å, and long-range electrostatics were treated using particle-mesh Ewald with periodic boundary conditions.

Upon trajectory stabilization, 100 snapshots were collected to calculate binding free energies between glycyrrhetinic acid and iNOS using the MM-PBSA method, including decomposition analysis to determine individual residue contributions.

Results and Discussion

UPLC-HRMS analysis of GC-derived components in GAHJ

GC comprises a diverse array of chemical constituents, many of which share structural similarities. To achieve optimal separation of these compounds, a Waters ACQUITY UPLC CSH C18 column was employed as the stationary phase, alongside carefully optimized mobile phase and elution conditions. The final LC setup utilized 0.1% formic acid in water (A) and 100% acetonitrile (B), which provided the most effective separation for

analysis. Using these optimized conditions, the high-resolution total ion chromatogram (TIC) of GAHJ was generated via UPLC-HRMS **(Figure 1)**.

A total of 193 GC-related compounds were detected in GAHJ. The structural characterization of these compounds was carried out using Compound Discoverer 3.1 software, combined with reference MS patterns and characteristic fragment ion information. Among the identified compounds, the structures of 139 were tentatively proposed, and 10—magnoflorine, liquiritin, ononin, daidzein, liquiritigenin, calycosin, formononetin, isoliquiritigenin, glycyrrhizin, and glycyrrhetinic acid were validated against authentic standards. Most of the 139 characterized compounds were classified as flavonoids or triterpenoid saponins.

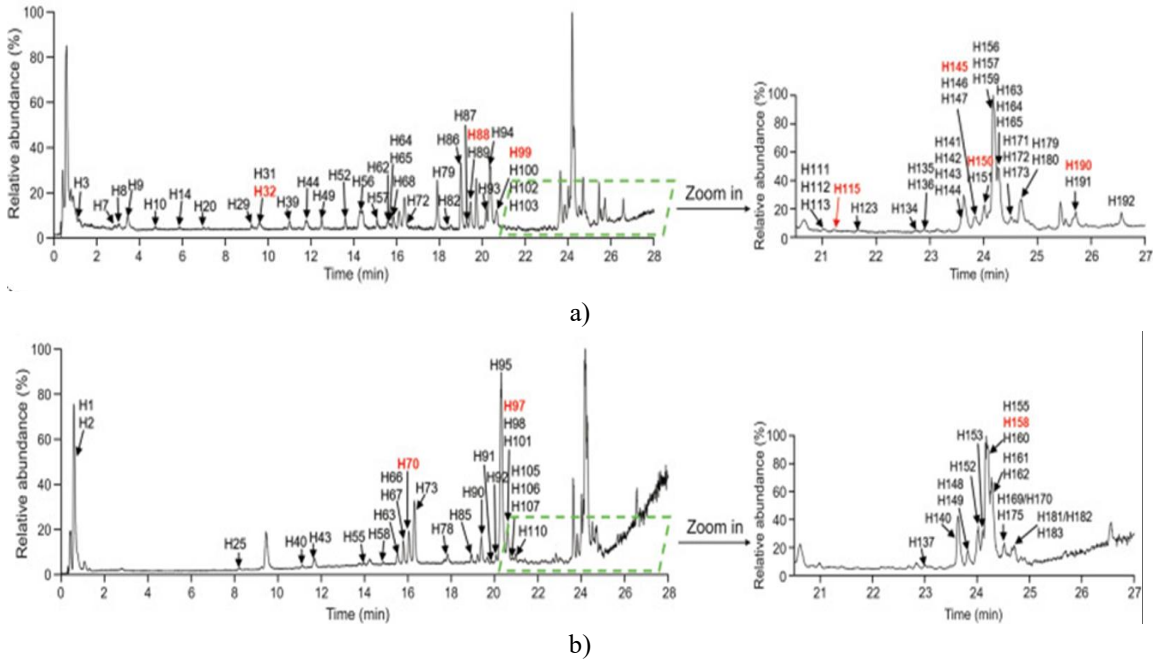

Figure 1. High-resolution total ion chromatograms (TIC) of Gan An He Ji oral liquid (GAHJ) analyzed by ultra-high performance liquid chromatography coupled with high-resolution mass spectrometry (UPLC-HRMS). (a) TIC in positive ion mode; (b) TIC in negative ion mode. Red numbers indicate compounds confirmed with reference standards.

Identification of GC-derived components exposed in humans

To investigate the in vivo exposure of GC-derived components, our team developed a comprehensive identification strategy for TCM constituents using advanced postprocessing tools for mass spectrometry (MS) data [17, 19, 34]. These methods include high-resolution extracted ion chromatograms, precise and thorough background subtraction (PATBS), mass defect filtering (MDF), data-independent acquisition product ion filters, as well as both targeted and untargeted analyses.

In this study, leveraging our previously established workflow [17], we conducted an extensive characterization of GC-related compounds detected in human samples. Representative results obtained with PATBS and MDF are presented in **Figure 2**. Compared to blank plasma **(Figure 2a)**, the raw chromatogram of human plasma after GAHJ administration **(Figure 2b)** contained multiple GC-related peaks but was dominated by endogenous components. Following PATBS processing, the plasma chromatograms became substantially cleaner, with endogenous interferences markedly reduced **(Figures 2c and 2d)**.

PATBS significantly simplified full-scan MS datasets, allowing for clear identification of individual GC components. For example, glycyrrhetinic acid appeared as a single molecular ion in the full-scan MS spectrum without notable interference **(Figure 2e)**. The mass spectral tree similarity filter (MTSF) was employed to automatically correlate metabolites with their corresponding prototype compounds based on spectral similarity. Additionally, the MDF technique helped determine whether detected GC-related components originated from parent compounds or from metabolite precursors, given that mass defect shifts of metabolites fall within predictable MDF windows.

Using a combination of MTSF and MDF, the relationships between GC metabolites observed in vivo and their corresponding prototype compounds were established, enabling evaluation of the biotransformation of major GC constituents. Specifically, MDF templates based on main GC prototype components **(Figure 2f)**, with glycyrrhetinic acid as the filter, allowed the elimination of endogenous interferences and facilitated the reconstruction of the metabolic pathways of GC components in humans. This approach also ensured that accurate MS/MS spectral data of GC constituents could be extracted from the recorded datasets. Structural elucidation of GC-related components was further supported by comparison with HRMS reference standards, GAHJ test solutions **(Figure 1)**, potential spectral interferences, and biotransformation patterns.

Through this comprehensive strategy, a total of 168 GC-related compounds were identified in humans, including 24 prototype compounds and 144 metabolites, with 135 detected in plasma and 82 in urine.

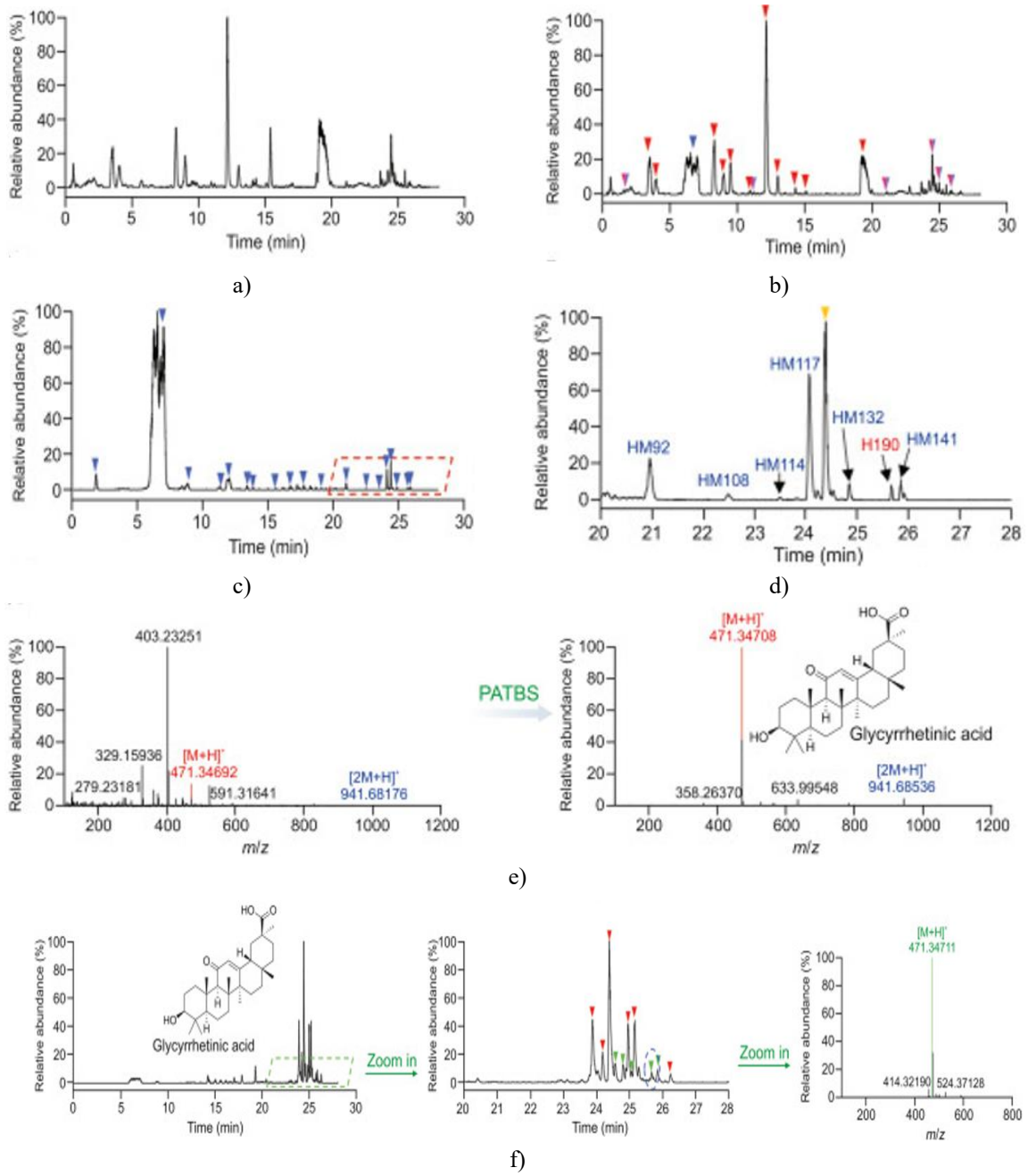

Figure 2. Characterization of Gan Cao (GC) constituents in human plasma using UPLC-HRMS (positive ion mode) with data processed by precise and thorough background subtraction (PATBS) and mass defect filtering (MDF). Full-scan MS chromatograms of (a) blank human plasma (pre-dose) and (b) plasma after GAHJ administration. (c) PATBS-processed chromatogram of the same plasma and (d) a partially enlarged

view. (e) Full-scan MS spectrum of glycyrrhetinic acid derived from PATBS-treated data. (f) MDF-processed chromatogram (±50 mDa).

Figures 3a and 3b display representative high-resolution TICs of GC-related compounds in human plasma and urine samples under positive and negative ion modes following repeated administration. **Figure 3c** illustrates the proportion of identified versus unidentified components. Compounds absorbed in vivo from TCM are generally considered the primary bioactive constituents, particularly those showing high exposure levels and favorable pharmacokinetic profiles.

In this study, 15 relatively high-exposure compounds were detected among the 130 GC-related components identified in humans **(Figure 3d)**. Metabolic transformation analysis revealed that these highly exposed components were derived from six key GC constituents: liquiritin (H70), liquiritigenin (H97), daidzein (H99), formononetin (H145), glycyrrhizin (H158), and glycyrrhetinic acid (H190). Collectively, the relative plasma and urine exposures of these six compounds and their metabolites accounted for 78% and 60%, respectively **(Figure 3e)**. **Figure 3f** depicts the metabolic pathways of these six components in humans following repeated administration.

Based on human exposure analysis, these six compounds represent the principal GC-related bioactive components in vivo. Considering their concentrations in GC—liquiritin (126.1 μg/mL), liquiritigenin (12.4 μg/mL), daidzein (37.1 μg/mL), formononetin (35.5 μg/mL), glycyrrhizin (1103.1 μg/mL), and glycyrrhetinic acid (25.1 μg/mL)—a potential active-component mixture comprising these six monomers was formulated for subsequent pharmacodynamic evaluation.

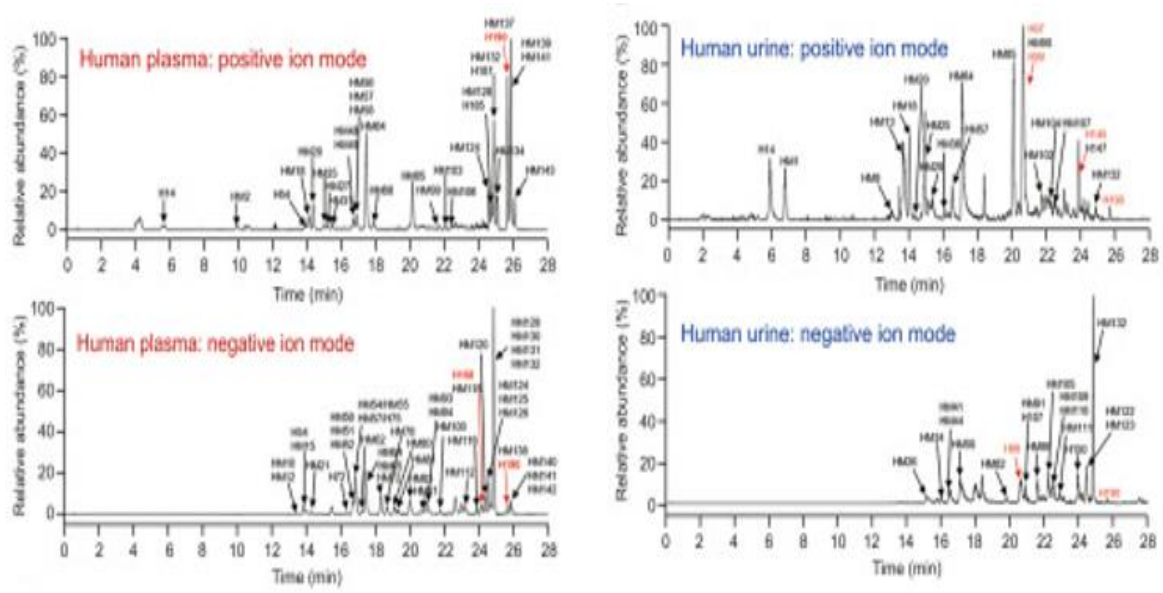

a) b)

c) d)

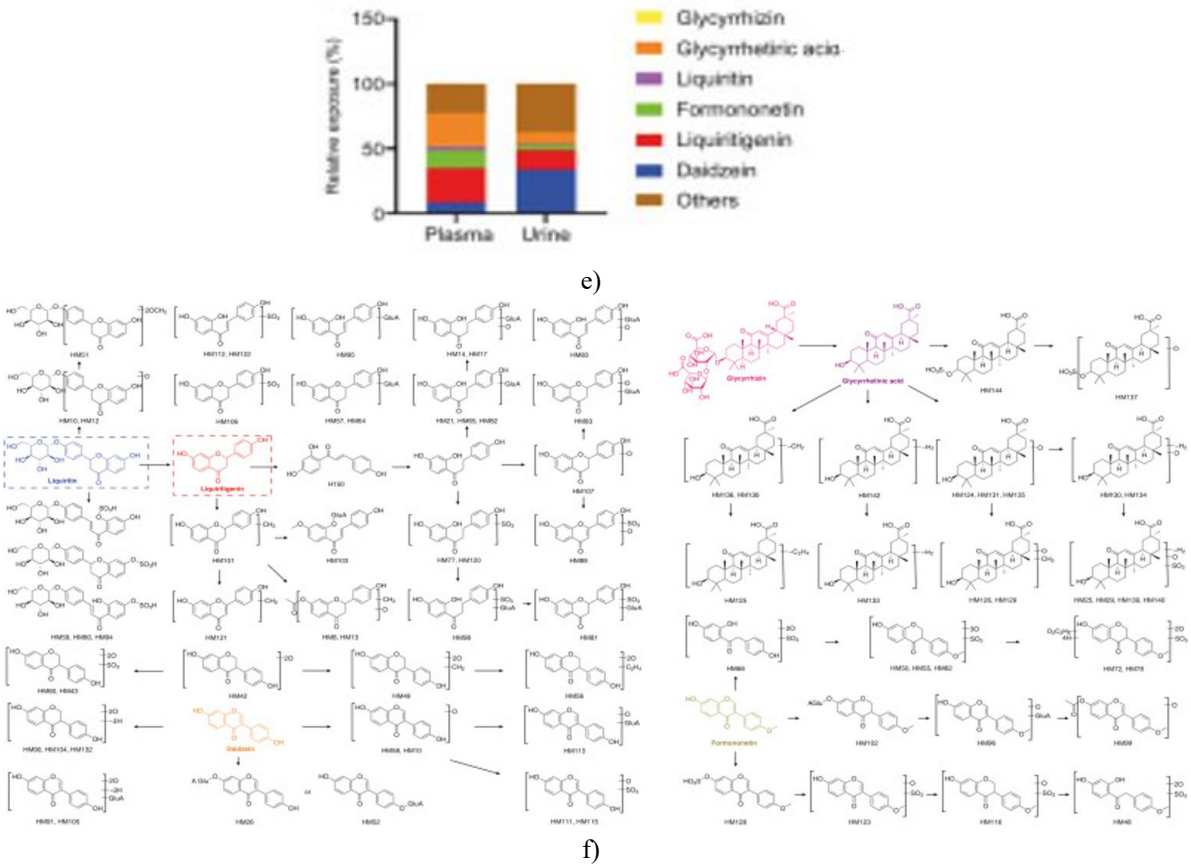

e)

f)

Figure 3. High-resolution total ion chromatograms (TIC) of Gan Cao (GC)-related compounds in biological samples following oral administration of Gan An He Ji (GAHJ), analyzed via UPLC-HRMS. (a) TIC of human plasma; (b) TIC of human urine in positive and negative ion modes; (c) proportion of identified versus unidentified GC components in vivo; (d) top 15 highly exposed compounds among the 130 GC-related components detected in plasma; (e) relative in vivo exposure of identified components in plasma and urine; (f) metabolic pathways of six key GC constituents (liquiritin, liquiritigenin, daidzein, formononetin, glycyrrhizin, and glycyrrhetinic acid) in humans. Red numbers indicate compounds confirmed with reference standards.

ADME metabolic profiling of GC-related components in rats

To further elucidate the absorption, distribution, metabolism, and excretion (ADME) characteristics of GC-related bioactive components and explore interspecies metabolic differences between humans and rats, we conducted an in-depth metabolic profiling study in rats following oral administration of GAHJ. Using our previously established ADME workflow for TCM [19, 34], a total of 210 GC-related compounds were identified in rats, comprising 86 prototype constituents and 124 metabolites. Of these, 147 compounds were detected in plasma, 109 in urine, 87 in feces, and 37 in bile.

Representative high-resolution TICs for rat plasma and urine in positive and negative ion modes after repeated administration are shown in **Figures 4a and 4b**, respectively. Based on these results, the in vivo ADME profile of GC-related components in rats was established. Flavonoids were primarily excreted as glucuronide conjugates but also underwent sulfation, oxidation, methylation, and other transformations **(Figure 4c)**. Triterpenoids predominantly underwent demethylation, sulfation, and glycoside hydrolysis, with glycoside removal serving as the main excretion pathway **(Figure 4d)**.

Overall, the metabolic profiles of GC-derived components in rats closely resembled those observed in human subjects with pneumonia, supporting the relevance and reliability of subsequent pharmacodynamic studies in rat models.

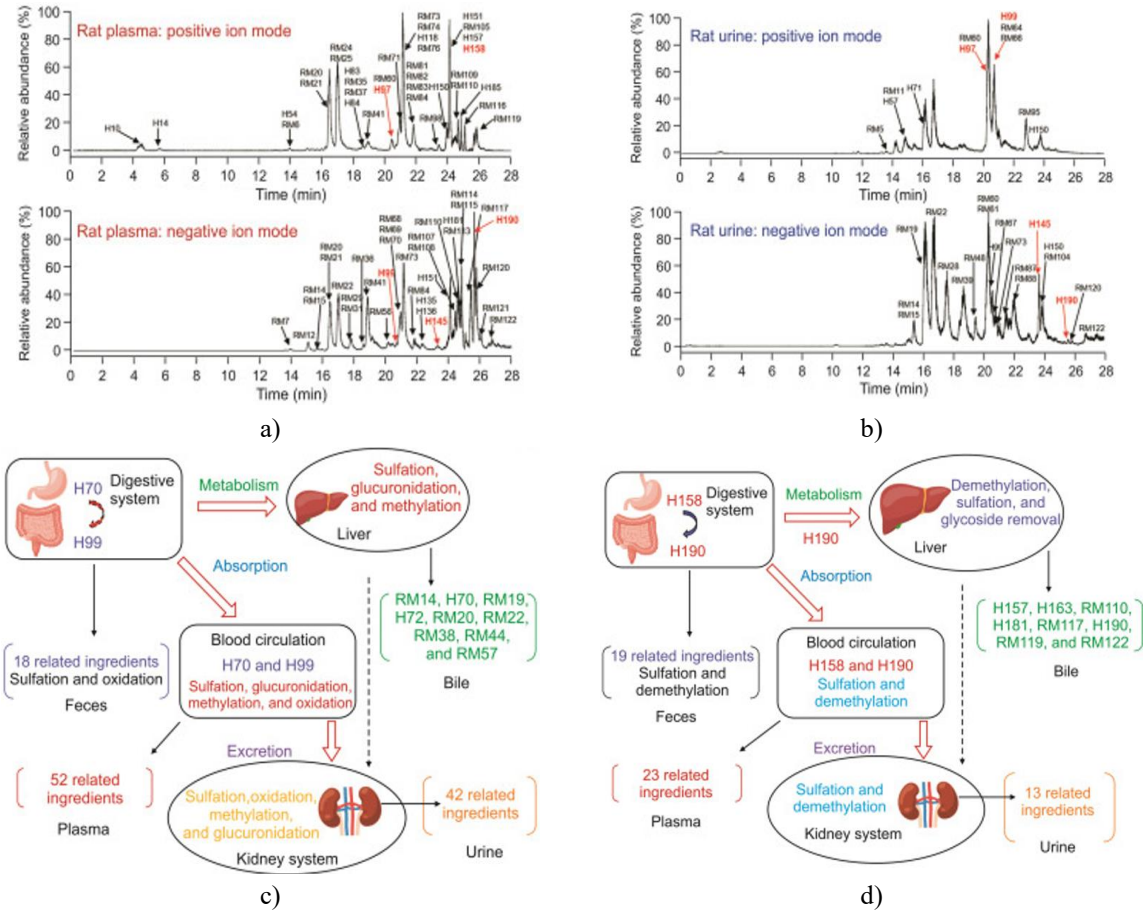

Figure 4. In vivo ADME profiles of representative Gan Cao (GC) components in rats. High-resolution total ion chromatograms of rat (a) plasma and (b) urine in both positive and negative ion modes. Red numbers indicate compounds confirmed using reference standards. (c) ADME characterization of flavonoids in GC, highlighting typical biotransformation reactions, with liquiritin and liquiritigenin as examples. (d) ADME characterization of triterpenoids in GC, including typical biotransformations, with glycyrrhizin and glycyrrhetinic acid as examples.

Network pharmacology and molecular docking of GC-derived active components

A compound-disease-target network was established by integrating potential GC-derived bioactive constituents with 100 key pneumonia-related targets. Among these, 50 targets were common to the six primary GC components. These 50 shared targets were subsequently analyzed using Kyoto Encyclopedia of Genes and Genomes (KEGG) pathway mapping and Gene Ontology enrichment. KEGG analysis revealed that most targets were involved in inflammatory and pneumonia-associated pathways, including the mitogen-activated protein kinase (MAPK) signaling cascade **(Figure 5)**.

From the network analysis, 12 targets with a degree greater than four were selected, and molecular docking was performed for 10 targets with available crystal structures in the Protein Data Bank (PDB). Docking results indicated that iNOS achieved the highest binding scores with liquiritigenin, glycyrrhetinic acid, daidzein, and formononetin. iNOS is a multifunctional signaling enzyme responsible for nitric oxide (NO) production [35, 36]. It plays a central role in mediating inflammatory responses by promoting the synthesis of proinflammatory cytokines such as interleukin-6 (IL-6) and IL-8 [37]. Excessive NO, superoxide, and other iNOS-derived inflammatory mediators can contribute to hemodynamic collapse in vivo, manifesting as increased vascular permeability, vasodilation, impaired tissue perfusion, and severe hypotension [38].

Therefore, targeting iNOS with specific inhibitors represents a promising strategy to mitigate cytokine storms and reduce inflammatory damage, providing a potential therapeutic approach for pneumonia. Based on network pharmacology and docking results, iNOS was identified as a key target for further experimental validation of the pharmacodynamic effects of GC-related compounds.

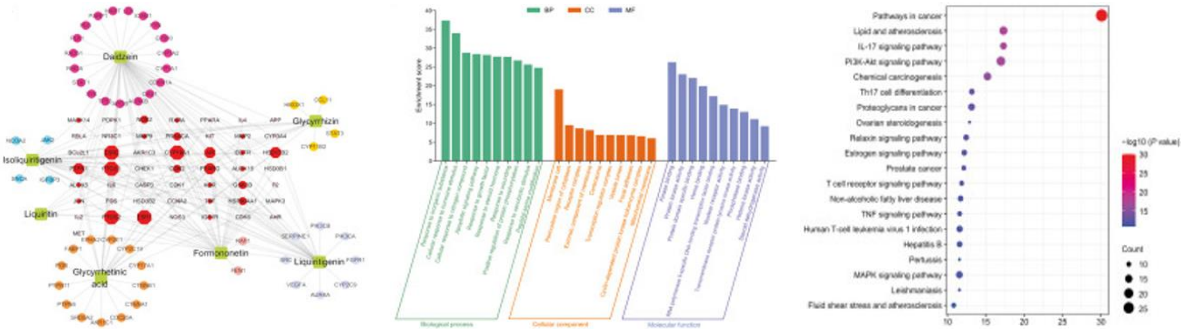

a) b) c)

Figure 5. Construction of the potential active component–key target network and enrichment analyses of Gene Ontology (GO) and Kyoto Encyclopedia of Genes and Genomes (KEGG) pathways. (a) Drug–target network established using potential active components of Gan An He Ji oral liquid (GAHJ) and 100 key proteins; (b) top 30 GO terms with $P < 0.01$; (c) top 20 KEGG pathways with $P < 0.05$. BP: biological processes; CC: cellular components; MF: molecular functions; IL: interleukin; PI3K-Akt: phosphatidylinositol 3-kinase-protein kinase B; Th17: T helper 17; TNF: tumor necrosis factor; MAPK: mitogen-activated protein kinase.

Therapeutic validation of GC-related components in an LPS-Induced mouse pneumonia model

The therapeutic potential of the GC-derived active-component complex, selected based on human in vivo exposure data, was assessed in an LPS-induced mouse model of pneumonia, with a focus on its modulatory effect on iNOS. **Figure 6a** illustrates the experimental design of the LPS-induced pneumonia model. qRT-PCR analysis revealed that iNOS mRNA expression was markedly elevated in the LPS group compared to the control (CON) group, whereas treatment with either the GC-derived active-component complex (LPS-Mix) or GAHJ (LPS-GAHJ) significantly reduced this upregulation **(Figure 6b)**.

ELISA results corroborated the PCR findings **(Figure 6c)**, showing that iNOS levels returned to near-normal following treatment with the active-component complex and GAHJ. Immunohistochemical analysis of lung tissues **(Figure 6d)**, quantified using ImageJ, displayed similar trends. The LPS group exhibited strong iNOS antigen expression in lung tissue, while the LPS-Mix and LPS-GAHJ groups showed substantial downregulation. These results collectively indicate that the GC-derived active-component complex effectively suppresses iNOS expression, which may contribute to the alleviation of pulmonary inflammation and improvement of lung function in this pneumonia model.

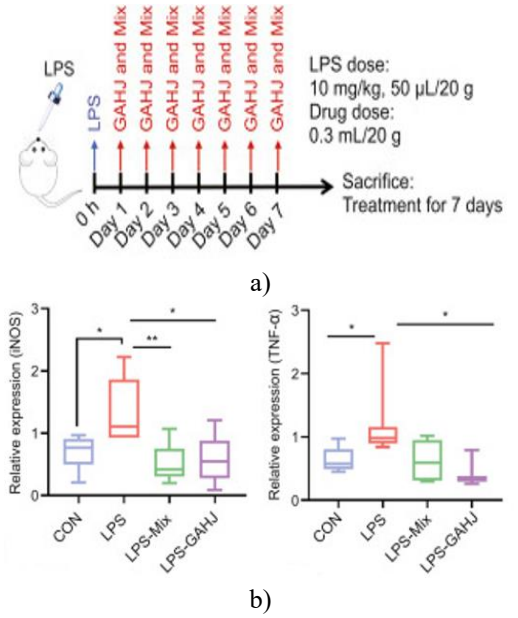

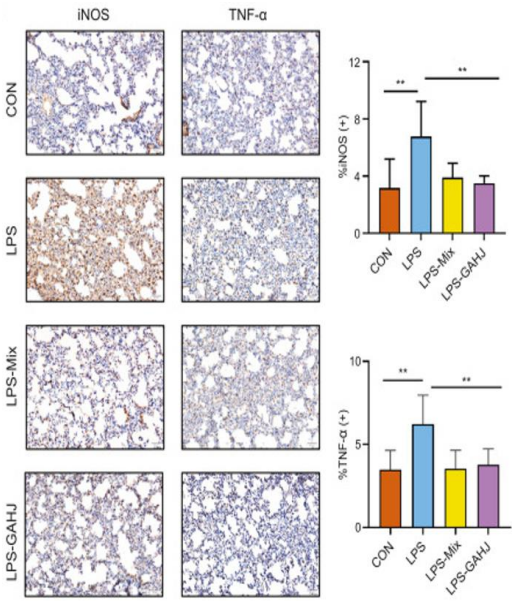

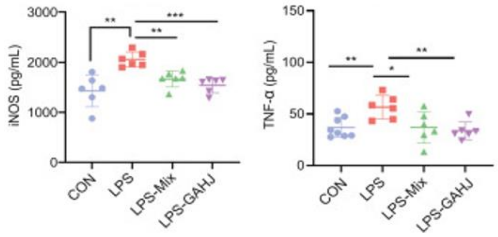

c) d)

Figure 6. GC-derived components, selected based on in vivo exposure in patients with pneumonia, effectively reduce inducible nitric oxide synthase (iNOS) expression and attenuate lung inflammation. (a) Experimental design of the lipopolysaccharide (LPS)-induced mouse pneumonia model; (b) lung tissue mRNA levels of iNOS and tumor necrosis factor (TNF)-α in the control (CON), LPS, LPS-Mix, and LPS-Gan An He Ji oral liquid (GAHJ) groups, measured by quantitative real-time PCR (n = 6); (c) plasma concentrations of iNOS and TNF-α in the same groups, determined by enzyme-linked immunosorbent assay (ELISA) (n = 6); (d) immunohistochemical staining of iNOS and TNF-α in lung tissues across groups (scale bar: 50 μm). (b–d) Data are shown as mean ± SEM (n = 6; ANOVA). ∗P < 0.05, ∗∗P < 0.01, ∗∗∗P < 0.001.

Therapeutic validation of GC-related components in a mouse model of S. aureus-induced pneumonia

To further confirm the regulatory effects of GC-derived active components on iNOS, a second pneumonia model was established using Staphylococcus aureus. **Figure 7a** depicts the experimental setup for this model. The results of qRT-PCR, ELISA, and immunohistochemistry were consistent with those observed in the LPS-induced model. Specifically, iNOS expression was markedly elevated in the S. aureus model group compared to the normal lung tissue (CON group). Treatment with either the S. aureus-Mix or S. aureus-GAHJ significantly suppressed iNOS levels, bringing them close to those observed in the CON group **(Figures 7b-7d)**.

These findings across two distinct pneumonia models confirm that the identified GC-related active components can robustly downregulate iNOS expression, demonstrating strong anti-inflammatory activity and improvement of pulmonary function. Importantly, this study provides the first evidence that the complex of GC-derived components exerts pharmacological effects comparable to the full GAHJ formulation in pneumonia treatment.

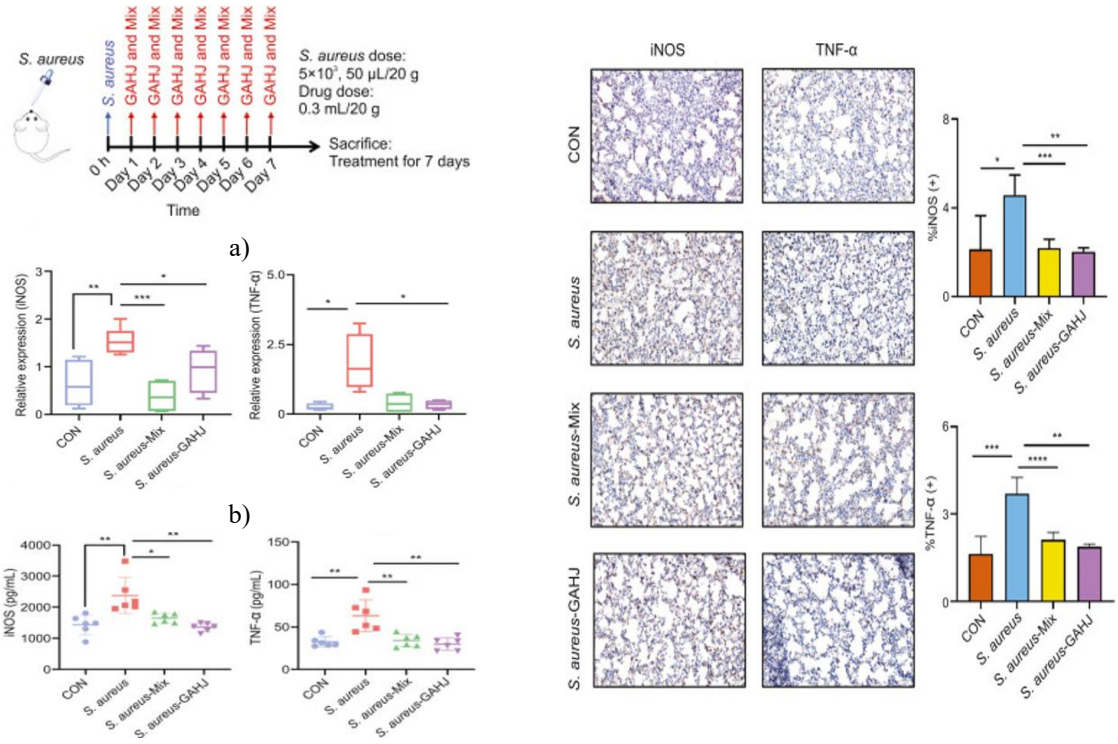

a) b) c) d)

Figure 7. The GC-derived components, selected based on their observed exposure in pneumonia patients, effectively reduced iNOS expression and mitigated lung inflammation in a mouse model of S. aureus-induced

pneumonia. (a) Illustration of the S. aureus-induced pneumonia model in mice. (b) Quantitative real-time PCR analysis of iNOS and TNF-α mRNA levels in lung tissues from the control (CON), S. aureus, S. aureus-Mix, and S. aureus-GAHJ groups (n = 6). (c) ELISA quantification of iNOS and TNF-α in plasma across the same experimental groups (n = 6). (d) Immunohistochemical staining of lung tissue showing iNOS and TNF-α distribution (scale bar: 50 μm). Data are expressed as mean ± SEM (n = 6, ANOVA). Statistical significance: ∗P < 0.05, ∗∗P < 0.01, ∗∗∗P < 0.001, ∗∗∗∗P < 0.0001.

Cellular evaluation and molecular dynamics of GC components targeting iNOS

The inhibitory activity of six major GC-derived components on iNOS was further assessed at the cellular level. Cytotoxicity assays **(Figure 8b)** determined the safe working concentrations for subsequent NOS activity measurements and WB analysis. Calculated IC50 values were: glycyrrhetinic acid, 45.53 μM; liquiritin, 2609.74 μM; daidzein, 1161.04 μM; liquiritigenin, 499.53 μM; glycyrrhizin, 1138.25 μM; and formononetin, 397.54 μM. Western blot results **(Figure 8c)** showed that 1400W (10 μM, a selective iNOS inhibitor), liquiritin (50 μM), liquiritigenin (50 μM), daidzein (12.5 μM), formononetin (5 μM), glycyrrhizin (12.5 μM), and glycyrrhetinic acid (10 μM) substantially suppressed iNOS protein levels. Corresponding NOS activity assays **(Figure 8d)** revealed that glycyrrhetinic acid maintained a robust inhibitory effect across different concentrations, with the most pronounced inhibition observed at 20 μM, exceeding that of the other compounds.

To further understand the interaction mechanism, a 100 ns molecular dynamics (MD) simulation of glycyrrhetinic acid bound to iNOS was conducted. Throughout the simulation, the ligand remained stably positioned at the binding site without inducing significant conformational changes in the protein or itself, confirming stable binding. The Binding free energy calculated via MM-PBSA and normal mode analysis was −17.74 kcal/mol, indicating a strong interaction. Residues contributing more than −0.5 kcal/mol were identified **(Figure 8e)**. Glycyrrhetinic acid established three hydrogen bonds with Gly371, Pro350, and Val352, while Met355, Ala262, Phe369, Trp463, and HEM contributed through significant van der Waals interactions.

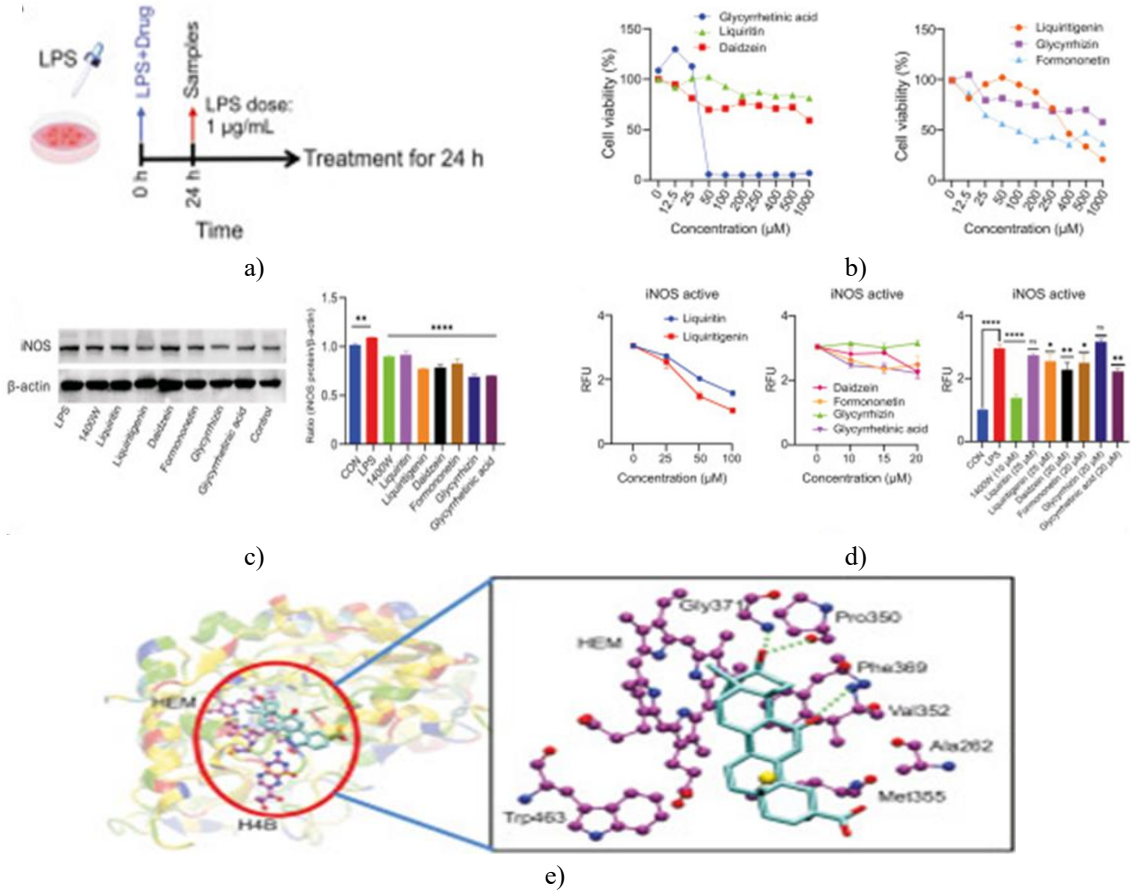

Figure 8. Evaluation of individual GC-derived active components in RAW264.7 cells. (a) Diagram of the LPS-induced RAW264.7 macrophage model; (b) cytotoxicity assay results of six monomeric compounds on

RAW264.7 cells (n = 6); (c) Western blot analysis showing the inhibitory effect of 1400W and the six monomers on iNOS protein expression; (d) NOS activity assay for 1400W and the six monomers (n = 2). Data in (c) and (d) are presented as mean ± SEM. Statistical significance: ∗P < 0.05, ∗∗P < 0.01, ∗∗∗P < 0.001, ∗∗∗∗P < 0.0001. (e) Molecular dynamics simulation of glycyrrhetinic acid binding to iNOS. Abbreviations: CON, control; RFU, relative fluorescence units; HEM, protoporphyrin IX containing Fe.

Traditional Chinese medicine (TCM) has been employed in China for over two millennia and remains a central component of the traditional pharmaceutical system. Understanding the chemical basis and therapeutic mechanisms of TCM has garnered significant attention from both drug discovery and clinical research. One of the primary challenges in TCM research is its inherent complexity, as it consists of hundreds of chemical constituents. Simplifying the composition by eliminating inactive compounds can enhance understanding and analysis.

In this study, we developed a systematic workflow to identify GC-related active components responsible for therapeutic effects in pneumonia and to predict their potential biological targets, guided by clinical human exposure data. Using nontargeted PATBS technology, GC-related components in GAHJ were initially identified, and MDF technology was subsequently applied to establish connections between parent compounds and their metabolites—key steps in our experimental design. While MTSF and MDF are traditionally applied to metabolite identification, here they were primarily used to map biotransformation pathways of the main GC components. The combined application of these intelligent MS data-mining tools—PATBS, MDF, and MTSF—greatly enhanced the efficiency and accuracy of detecting, identifying, and analyzing GC-related compounds in vivo.

The workflow consisted of five major steps. First, UPLC-HRMS analysis of the GAHJ solution allowed the identification of 193 GC-related compounds, of which 139 were structurally characterized, and 10 were confirmed against reference standards, providing essential structural information for subsequent in vivo experiments. Second, integrating UPLC-HRMS with advanced postprocessing MS data techniques enabled the identification and characterization of 168 GC-related compounds in plasma from pneumonia patients, establishing the biotransformation relationships among them. From this dataset, six highly exposed components—liquiritin, liquiritigenin, daidzein, formononetin, glycyrrhizin, and glycyrrhetinic acid—were selected for further evaluation in pneumonia models, both individually and as a combined mixture. Additionally, ADME profiling in rats revealed 210 GC-related components (86 prototypes and 124 metabolites), providing detailed insights into the metabolic clearance of these compounds and highlighting species-specific differences in metabolism.

Third, network pharmacology and molecular docking analyses identified iNOS as a key target protein mediating the therapeutic effects of these GC-related components. Fourth, the efficacy of the selected components and their mixture was validated in LPS- and S. aureus-induced mouse pneumonia models, confirming their ability to regulate iNOS expression and attenuate pulmonary inflammation. Finally, the effect of each individual component on iNOS was assessed in RAW264.7 cells, demonstrating that glycyrrhetinic acid exerted the strongest pharmacodynamic activity. Molecular dynamics simulations further revealed stable binding of glycyrrhetinic acid to iNOS, with detailed interaction patterns and binding free energy analysis.

iNOS is a critical mediator in inflammatory and infectious responses, producing nitric oxide (NO) as part of the host immune defense. Excessive NO production, primarily induced by iNOS in alveolar epithelial cells, bronchial cells, infiltrating leukocytes, and alveolar macrophages, contributes to lung inflammation. Therefore, inhibition of iNOS by the identified GC components can reduce inflammatory injury and improve pulmonary function, supporting their potential therapeutic role in pneumonia management [39, 40].

In this study, we demonstrated that the principal components of GC, particularly glycyrrhetinic acid, possess notable anti-inflammatory properties, and it is likely that some of their metabolites exert similar effects. Exploring metabolites as potential sources of new therapeutic agents represents an important strategy in drug discovery. However, due to the limitations of LC-MS in metabolite identification, many metabolites could not be accessed for subsequent in vitro or in vivo validation. A detailed examination of the chemical structures of the identified metabolites, particularly those derived from glycyrrhetinic acid, revealed that sulfation, oxidation, and demethylation were the predominant in vivo transformations. Given the structural similarity to the parent compounds, these metabolites are expected to maintain comparable anti-inflammatory activity. Nevertheless, confirming this hypothesis will require future medicinal chemistry studies, including the chemical synthesis of these metabolites. Additionally, structural optimization could be pursued to enhance their pharmacological activity and drug-like properties, which will be addressed in our future research.

Conclusion

In summary, UPLC-HRMS was employed to systematically investigate the in vivo exposure and metabolism of GC, while advanced MS data postprocessing technologies, including PATBS, MDF, and MTSF, were used to enhance the efficiency of identifying complex TCM components in biological samples. From the perspective of clinical exposure in pneumonia patients, six GC-related active components—liquiritin, liquiritigenin, daidzein, formononetin, glycyrrhizin, and glycyrrhetinic acid—were successfully identified as potential therapeutic agents for pneumonia. For the first time, our findings indicate that iNOS may serve as a critical target through which GC-related components exert their anti-pneumonia effects. This conclusion was further supported by validations in pneumonia animal models and cellular assays, which confirmed that GC alleviates pulmonary inflammation and improves lung function via iNOS modulation. Among the six active compounds, glycyrrhetinic acid exhibited the strongest regulatory effect and the highest exposure in human subjects. To our knowledge, this is the first report detailing the in vivo exposure of pneumonia patients to GC-related components. Overall, these results provide compelling evidence for identifying key bioactive constituents of GC and elucidating their potential mechanisms in pneumonia prevention and treatment, offering a scientific basis for its clinical application.

Acknowledgments: None

Conflict of Interest: None

Financial Support: None

Ethics Statement: None

References

1. Liu H, Wang J, Zhou W, Wang Y, Yang L. Systems approaches and polypharmacology for drug discovery from herbal medicines: an example using licorice. J Ethnopharmacol. 2013;146(3):773-93.
2. Sun HX, Pan HJ. Immunological adjuvant effect of Glycyrrhiza uralensis saponins on the immune responses to ovalbumin in mice. Vaccine. 2006;24(11):1914-20.
3. Jiang M, Zhao S, Yang S, Lin X, He X, Wei X, et al. An "essential herbal medicine"-licorice: A review of phytochemicals and its effects in combination preparations. J Ethnopharmacol. 2020;249:112439.
4. Wang L, Yang R, Yuan B, Liu Y, Liu C. The antiviral and antimicrobial activities of licorice, a widely-used Chinese herb. Acta Pharm Sin B. 2015;5(4):310-5.
5. Wang Y, Zhang X, Ma X, Zhang K, Li S, Wang X, et al. Study on the kinetic model, thermodynamic and physicochemical properties of Glycyrrhiza polysaccharide by ultrasonic assisted extraction. Ultrason Sonochem. 2019;51:249-57.
6. Yang R, Wang LQ, Yuan BC, Liu Y. The pharmacological activities of licorice. Planta Med. 2015;81(18):1654-69.
7. Yu JY, Ha JY, Kim KM, Jung YS, Jung JC, Oh S. Anti-Inflammatory activities of licorice extract and its active compounds, glycyrrhizic acid, liquiritin and liquiritigenin, in BV2 cells and mice liver. Molecules. 2015;20(7):13041-54.
8. Ramalingam M, Kim H, Lee Y, Lee YI. Phytochemical and pharmacological role of liquiritigenin and isoliquiritigenin from radix glycyrrhizae in human health and disease models. Front Aging Neurosci. 2018;10:348.
9. Pandit S, Ponnusankar S, Bandyopadhyay A, Ota S, Mukherjee PK. Exploring the possible metabolism mediated interaction of Glycyrrhiza glabra extract with CYP3A4 and CYP2D6. Phytother Res. 2011;25(10):1429-34.
10. Fukai T, Marumo A, Kaitou K, Kanda T, Terada S, Nomura T. Anti-Helicobacter pylori flavonoids from licorice extract. Life Sci. 2002;71(12):1449-63.
11. Reuter J, Merfort I, Schempp CM. Botanicals in dermatology: an evidence-based review. Am J Clin Dermatol. 2010;11(4):247-67.

12. Luo L, Jiang J, Wang C, Fitzgerald M, Hu W, Zhou Y, et al. Analysis on herbal medicines utilized for treatment of COVID-19. Acta Pharm Sin B. 2020;10(7):1192-204.
13. Xian Y, Zhang J, Bian Z, Zhou H, Zhang Z, Lin Z, et al. Bioactive natural compounds against human coronaviruses: a review and perspective. Acta Pharm Sin B. 2020;10(7):1163-74.
14. Zhao J, Tian S, Lu D, Yang J, Zeng H, Zhang F, et al. Systems pharmacological study illustrates the immune regulation, anti-infection, anti-inflammation, and multi-organ protection mechanism of Qing-Fei-Pai-Du decoction in the treatment of COVID-19. Phytomedicine. 2021;85:153315.
15. Liu J, Yang W, Liu Y, Lu C, Ruan L, Zhao C, et al. Combination of Hua Shi Bai Du granule (Q-14) and standard care in the treatment of patients with coronavirus disease 2019 (COVID-19): A single-center, open-label, randomized controlled trial. Phytomedicine. 2021;91:153671.
16. Huang YF, Bai C, He F, Xie Y, Zhou H. Review on the potential action mechanisms of Chinese medicines in treating Coronavirus Disease 2019 (COVID-19). Pharmacol Res. 2020;158:104939.
17. Chen X, Wu Y, Chen C, Gu Y, Zhu C, Wang S, et al. Identifying potential anti-COVID-19 pharmacological components of traditional Chinese medicine Lianhuaqingwen capsule based on human exposure and ACE2 biochromatography screening. Acta Pharm Sin B. 2021;11(1):222-36.
18. van de Sand L, Bormann M, Alt M, Schipper L, Heilingloh CS, Steinmann E, et al. Glycyrrhizin effectively inhibits SARS-CoV-2 replication by inhibiting the viral main protease. Viruses. 2021;13(4):609.
19. Zhu C, Cai T, Jin Y, Chen J, Liu G, Xu N, et al. Artificial intelligence and network pharmacology based investigation of pharmacological mechanism and substance basis of Xiaokewan in treating diabetes. Pharmacol Res. 2020;159:104935.
20. Wang X, Zhang A, Zhou X, Liu Q, Nan Y, Guan Y, et al. An integrated chinmedomics strategy for discovery of effective constituents from traditional herbal medicine. Sci Rep. 2016;6:18997.
21. Chen T, Wang X, Chen P, Zheng Y, He Y, Zeng X, et al. Chemical components analysis and in vivo metabolite profiling of Jian'er Xiaoshi oral liquid by UHPLC-Q-TOF-MS/MS. J Pharm Biomed Anal. 2022;211:114629.
22. Dong W, Wang P, Meng X, Sun H, Zhang A, Wang W, et al. Ultra-performance liquid chromatography-high-definition mass spectrometry analysis of constituents in the root of Radix Stemonae and those absorbed in blood after oral administration of the extract of the crude drug. Phytochem Anal. 2012;23(6):657-67.
23. Shi J, Wang H, Liu J, Zhang Y, Luo J, Li Y, et al. Ganoderic acid B attenuates LPS-induced lung injury. Int Immunopharmacol. 2020;88:106990.
24. Wu Q, Li H, Qiu J, Feng H. Betulin protects mice from bacterial pneumonia and acute lung injury. Microb Pathog. 2014;75:21-8.
25. Kapetanovic R, Jouvion G, Fitting C, Parlato M, Blanchet C, Huerre M, et al. Contribution of NOD2 to lung inflammation during Staphylococcus aureus-induced pneumonia. Microbes Infect. 2010;12(10):759-67.
26. Jones G, Willett P, Glen RC, Leach AR, Taylor R. Development and validation of a genetic algorithm for flexible docking. J Mol Biol. 1997;267(3):727-48.
27. Yoon HJ, Moon ME, Park HS, Im SY, Kim YH. Chitosan oligosaccharide (COS) inhibits LPS-induced inflammatory effects in RAW 264.7 macrophage cells. Biochem Biophys Res Commun. 2007;358(3):954-9.
28. Hwang SJ, Kim YW, Park Y, Lee HJ, Kim KW. Anti-inflammatory effects of chlorogenic acid in lipopolysaccharide-stimulated RAW 264.7 cells. Inflamm Res. 2014;63(1):81-90.
29. Garcin ED, Arvai AS, Rosenfeld RJ, Kroeger MD, Crane BR, Andersson G, et al. Anchored plasticity opens doors for selective inhibitor design in nitric oxide synthase. Nat Chem Biol. 2008;4(11):700-7.
30. Kang S, Tang W, Li H, Chreifi G, Martásek P, Roman LJ, et al. Nitric oxide synthase inhibitors that interact with both heme propionate and tetrahydrobiopterin show high isoform selectivity. J Med Chem. 2014;57(10):4382-96.
31. Kolodziejski PJ, Rashid MB, Eissa NT. Intracellular formation of "undisruptable" dimers of inducible nitric oxide synthase. Proc Natl Acad Sci U S A. 2003;100(24):14263-8.
32. Perry JM, Marletta MA. Effects of transition metals on nitric oxide synthase catalysis. Proc Natl Acad Sci U S A. 1998;95(19):11101-6.
33. Hong W, Wang Y, Chang Z, Yang Y, Pu J, Sun T, et al. The identification of novel Mycobacterium tuberculosis DHFR inhibitors and the investigation of their binding preferences by using molecular modelling. Sci Rep. 2015;5:15328.

34. Wu C, Zhang H, Wang C, Qin H, Zhu M, Zhang J. An integrated approach for studying exposure, metabolism, and disposition of multiple component herbal medicines using high-resolution mass spectrometry and multiple data processing tools. Drug Metab Dispos. 2016;44(6):800-8.
35. Gross TJ, Kremens K, Powers LS, Brink B, Knutson T, Domann FE, et al. Epigenetic silencing of the human NOS2 gene: rethinking the role of nitric oxide in human macrophage inflammatory responses. J Immunol. 2014;192(5):2326-38.
36. Wang X, Gray Z, Willette-Brown J, Zhu F, Shi G, Jiang Q, et al. Macrophage inducible nitric oxide synthase circulates inflammation and promotes lung carcinogenesis. Cell Death Discov. 2018;4:46.
37. Vuolteenaho K, Koskinen A, Kukkonen M, Nieminen R, Päivärinta U, Moilanen T, et al. Leptin enhances synthesis of proinflammatory mediators in human osteoarthritic cartilage--mediator role of NO in leptin-induced PGE2, IL-6, and IL-8 production. Mediators Inflamm. 2009;2009:345838.
38. Feitosa EL, Júnior FTDSS, Nery Neto JAO, Matos LFL, Moura MHS, Rosales TO, et al. COVID-19: rational discovery of the therapeutic potential of Melatonin as a SARS-CoV-2 main protease inhibitor. Int J Med Sci. 2020;17(14):2133-46.
39. Coleman JW. Nitric oxide in immunity and inflammation. Int Immunopharmacol. 2001;1(8):1397-406.
40. Okamoto T, Gohil K, Finkelstein EI, Bove P, Akaike T, van der Vliet A. Multiple contributing roles for NOS2 in LPS-induced acute airway inflammation in mice. Am J Physiol Lung Cell Mol Physiol. 2004;286(1):L198-209.